Adaptive geometric numerical integration for point vortex dynamics

A. San Miguel*

Departamento de Matemática Aplicada, Universidad de Valladolid Facultad de Ciencias, Prado de la Magdalena s/n, 47005 Valladolid, Spain

(Received 7 March 2006; revised manuscript received 26 July 2006; published 18 October 2006)

In this paper we describe a variable stepsize integration method for the Hamiltonian dynamics of point vortices based on the explicit symplectic Zhang and Qin scheme. The adapted method is also explicit and preserves the reversible structure of the flow. In order to check the behavior of this adaptive method a numerical study of the exchange-scattering phenomenon in the three-vortex problem is made. The symmetry of the orbit and the energy evolution are discussed for the exchange-scattering model. A long-term integration of this and other models composed also of three vortices indicates that the adaptive Zhang-Qin method has good properties of efficiency and preservation of the first integrals associated with point vortex systems.

DOI: 10.1103/PhysRevE.74.046706 PACS number(s): 47.11.−j, 47.32.C−

I. INTRODUCTION

Numerical techniques for the treatment of complex systems in point vortex dynamics have been successfully employed in numerous problems over the last two decades. So, for example, numerical experiments using classical integrators was used to give evidence of chaos in the four-vortex problem by Aref and Pomphrey [1,2] or more recently in the study of the transport of tracers particles in a three-vortex flow by Kuznetsov and Zaslavsky [3].

On the other hand, the theory of numerical methods that preserve geometric properties of the flow of a differential equation, for example the symplectic structure for Hamiltonian systems, provides stable methods for long time interval simulations. This subject is treated in the work of Sanz-Serna and Calvo [4], and in more recent works by Hairer, Lubich, and Wanner [5] and Leimkuhler and Reich [6]. In the context of vortex dynamics Pullin and Saffman [7] found that a symplectic scheme of the implicit Runge-Kutta type gives a superior performance over the explicit Runge-Kutta scheme, which is not symplectic, when both are applied to very long integration times in the motion of four identical point vortices. Another comparison between symplectic and classical schemes for this system vortex may be found in Boatto and Pierrehumbert [8].

An efficient explicit symplectic method for point vortex systems was proposed by Zhang and Qin [16] using a splitting of the Hamiltonian function as a sum of the Hamiltonians corresponding to integrable systems constituted by two vortices. In addition, geometric methods for the point vortex dynamics have also been developed from different approaches. For example, Rowley and Marsden [9] have constructed a variational integrator for the degenerate Lagrangian system corresponding to N vortices, and Newton and Kushalani [10] have applied a decomposition method into all possible subclusters in a system of N-point vortices, where each subcluster of vortices is completely integrable.

To obtain a numerical solution of certain problems it is useful to control the stepsize in order to reduce computational cost, but in doing so it turns out (cf. [5], and references therein) that the good behavior of symplectic methods is destroyed if ordinary stepsize strategies are applied. Even so, several attempts have been made to construct geometric adaptive integrators, [11–14]. In one of these approaches, Refs. [13,14], an explicit variable stepsize modification of the Störmer-Verlet discretization is obtained introducing a time reparametrization by means of a Sundman transformation. This technique has proved efficient in the treatment of perturbed Kepler motion by Leimkuhler [15]. Instead of the symplectic structure, in these adaptive discretizations the geometric structure which one tries to preserve is the time reversibility of the dynamical system for which it is well known (see, e.g., Ref. [17]) that important properties of Hamiltonian systems, such as the existence of the Kolmogorov-Arnol'd-Moser tori, are shared by reversible systems.

The aim of the present paper is to construct an adaptive geometric integrator for the motion of N vortices by applying a time parametrization based on the Zhang-Qin scheme. For this, in Sec. II we outline the theory behind the motion of point vortices. Particular attention is paid to the Hamiltonian structure and the time reversibility of point vortex dynamics. The numerical integration of this Hamiltonian system by the Zhang-Qin method is also briefly treated. Section III presents an adaptive explicit method which preserves the time reversibility of the flow. The resulting algorithm is second order, explicit and time reversible and a higher order method is obtained by a composition technique.

In Sec. IV, the adaptive method is applied to the integration of a model in which an exchange scattering of a neutral pair by a simple vortex occurs, as that studied by Aref [18]. The property of the preservation of the energy and the symmetry of the orbit of this dynamical system is discussed for different choices of the scaling function used in the time parametrization. Also a Scovel projection of the adapted method is applied in order to obtain another method which is time reversible under an involution which takes into account the exchange of vortices. This modification gives a better behavior of the energy deviation in the exchange-scattering model considered. Finally, in Sec. V, a long-term integration for various three-vortex models is made. We compare the efficiency of the adaptive method and the corresponding

*Electronic address: asmiguel@maf.uva.es

fixed stepsize method. Furthermore, the preservation properties of the linear and angular impulses are also studied.

II. THE DYNAMICAL SYSTEM

A. Equations of motion

The description of the dynamics of a three-dimensional vortex system whose vortex tubes are almost straight and parallel may be modeled through a system of point vortices moving in a two-dimensional ideal fluid to which the Euler equation and Helmholtz's vorticity theorems are applicable. An even more simplified model is obtained assuming a singular vorticity distribution everywhere zero except on N points, $V_1, V_2, \ldots, V_N$, in the plane, $\omega := \sum_{i=1}^{N} \kappa_i \delta(\boldsymbol{r}-\boldsymbol{r}_i)$ (see [21], Ch. 7), where κ_i is the strength of each vortex; $\boldsymbol{r} = (x,y) \in \mathbb{R}^2$ is a generic point in the plane; $\boldsymbol{r}_i = (x_i, y_i)$ is the position of the ith vortex, and δ is the Dirac distribution supported by the point $\boldsymbol{r}_i$. The reduction from a continuum model to another discrete makes that the evolution equations change from the partial differential equation given by Euler to an ordinary differential equation as it is described in classical textbooks (see [22]). After this reduction, the velocity of the vortex of strength κ_i coincides with the velocity of the flow at the point (x_i, y_i) due to all other vortices:

$$\dot{x}_j = -\frac{1}{2\pi} \sum_{i(\neq j)} \kappa_i \frac{y_j - y_i}{r_{ij}^2}, \quad \dot{y}_j = \frac{1}{2\pi} \sum_{i(\neq j)} \kappa_i \frac{x_j - x_i}{r_{ij}^2}, \tag{1}$$

where $j = 1, \ldots, N$ and $r_{ij} = \|\boldsymbol{r}_i - \boldsymbol{r}_j\|$.

The differential system (1) has four independent first integrals

$$X := \sum \kappa_i x_i, \quad Y := \sum \kappa_i y_i,$$

$$I := \sum \kappa_i \|\boldsymbol{r}_i\|^2, \quad H := \frac{1}{4\pi} \sum_{i(\neq j)} \kappa_i \kappa_j \ln r_{ij}^2, \tag{2}$$

related to the preservation of the vortex center, angular momentum, and kinetic energy (see, e.g., Ref. [19]).

The equation of motion (1) can be described as a dynamical system on the phase space

$$\mathcal{M} := \{\boldsymbol{q} \in \mathbb{R}^{2N} | (q_i, q_{i+N}) \neq (q_j, q_{j+N}), \quad \text{if } i \neq j\}, \tag{3}$$

where $q_i := x_i$, $i = 1, \ldots, N$, are the generalized coordinates and $q_{i+N} := y_i$ the generalized momenta. In that case the first integral H defined in (2) is interpreted as a real function on $\mathcal{M}$:

$$H(\boldsymbol{q}) := -\frac{1}{4\pi} \sum_{i(\neq j)} \kappa_i \kappa_j \ln((q_i - q_j)^2 + (q_{i+N} - q_{j+N})^2). \tag{4}$$

Using this notation, Eq. (1) is equivalent to the noncanonical Hamiltonian system

$$\dot{\boldsymbol{q}} = X(\boldsymbol{q}), \quad \text{with } X(\boldsymbol{q}) := \mathbb{B}\, \text{grad}\, H(\boldsymbol{q}), \tag{5}$$

where $\mathbb{B}$ is the skew-symmetric invertible $2N \times 2N$ matrix

$$\mathbb{B} := \begin{pmatrix} \boldsymbol{0} & \boldsymbol{A} \\ -\boldsymbol{A} & \boldsymbol{0} \end{pmatrix}, \quad \boldsymbol{A} := \text{diag}(\kappa_1^{-1}, \ldots, \kappa_N^{-1}). \tag{6}$$

Observe that under an involution $\varrho : \mathcal{M} \to \mathcal{M}$ (i.e., a map ϱ such that $\varrho^2 = \text{Id}$) of the form $\varrho : \boldsymbol{q} \mapsto \bar{\boldsymbol{q}}$, with

$$\bar{q}_i = q_i, \quad \bar{q}_{i+N} = -q_{i+N}, \quad (i = 1, \ldots, N), \tag{7}$$

the Hamiltonian remains invariant: $H \circ \varrho = H$. So, the Hamiltonian system (5) is reversible and the vector field $X(\boldsymbol{q})$ satisfies the ϱ-reversibility condition (see Ref. [17])

$$X(\boldsymbol{q}) = -\varrho \circ X \circ \varrho(\boldsymbol{q}). \tag{8}$$

B. Numerical integration

The Zhang-Qin scheme [16] is an explicit numerical method for the integration of the equation of motion of a system of N-point vortices. It is based on the splitting of the Hamiltonian function in the form

$$H = \sum_{a=1}^{\nu} H_a, \quad \text{with } \nu := \binom{N}{2}, \tag{9}$$

where each H_a is the Hamiltonian for a pair of vortices. Since in the Hamiltonian H_a corresponding to two vortices V_i, V_j the function r_{ij} remains constant along the motion, each differential equation $\dot{\boldsymbol{q}} = \mathbb{B}\, \text{grad}\, H_a$ reduces to a differential system with constant coefficients for which the solution corresponding to an initial value $\boldsymbol{q}(0) =: \boldsymbol{q}_0$ may be expressed in terms of elementary functions. Let us denote by $\varphi_t^{[a]}$ the flow on $\mathcal{M}$ corresponding to the vector field $X^{[a]} := \mathbb{B}\, \text{grad}\, H_a$ (see Appendix A1 for a matrix representation of $\varphi_t^{[a]}$).

Now, let us consider a discretization of both time and position in the phase space:

$$t_n = nh, \quad \boldsymbol{q}_n := \boldsymbol{q}(t_n), \tag{10}$$

where h is a constant stepsize and $n \in \{0, 1, 2, \ldots\}$. The map $\varphi_{-h}^{[a]}$ is given by the matrix derived from (A2) replacing b_1 and b_2 by $-b_1$ and $-b_2$, respectively. Therefore, the reversibility condition under the involution ϱ is satisfied:

$$\varrho \circ \varphi_h^{[a]} \circ \varrho = \varphi_{-h}^{[a]}. \tag{11}$$

We also note that since $\varphi_h^{[a]}$ is an exact flow, it is time symmetric (cf. e.g., Ref. [5], p. 38):

$$\varphi_{-h}^{[a]} = (\varphi_h^{[a]})^{-1}, \tag{12}$$

so that considering $\varphi_h^{[a]}$ as a numerical integrator, this coincides with its adjoint defined as $(\varphi_h^{[a]})^* := (\varphi_{-h}^{[a]})^{-1}$.

By composition of the partial maps $\varphi_h^{[a]}$,

$$\boldsymbol{q}_{n+1} = \phi_h(\boldsymbol{q}_n) := \varphi_h^{[1]} \circ \cdots \circ \varphi_h^{[\nu]}(\boldsymbol{q}_n), \tag{13}$$

one can derive a first order symplectic method, $\phi_h : \boldsymbol{q}_n \mapsto \boldsymbol{q}_{n+1}$, for the N-vortex motion. Furthermore, from the time symmetry of φ_h, the adjoint method, $\phi_h^* = (\phi_{-h})^{-1}$, associated to ϕ_h may be found as follows:

$$\phi_h^* := \varphi_h^{[\nu]} \circ \cdots \circ \varphi_h^{[1]}. \tag{14}$$

Then the map

$$\Phi_h := \phi^*_{h/2} \circ \phi_{h/2} \tag{15}$$

gives the second order method due to Zhang and Qin [16].

It is interesting to observe that, due to properties (11) and (12), the integrator Φ_h is reversible under involution (8):

$$\varrho \circ \Phi_h \circ \varrho = \Phi_{-h}, \tag{16}$$

and it is also time symmetric

$$\Phi_h^{-1} = \Phi_{-h}. \tag{17}$$

The integrator Φ_h preserves the symplectic structure (6) and consequently has a good behavior when applied to a long-term integration.

III. ADAPTIVE ZHANG-QIN METHOD

For the integration of some problems (as that treated in the next section) it may be useful to introduce a stepsize control in the Zhang-Qin scheme in order to increase the efficiency of the method. But as it is known (see [4]) the variation of the stepsize makes a symplectic integrator lose the original good properties of preservation of the energy.

However, an efficient geometrical integrator with variable stepsize may even be constructed. One approach to variable stepsize integration based on the Störmer-Verlet method was established in [20] for the N-body problem in celestial and molecular dynamics. In this method a numerical discretization is made so that the time reversibility of the flow is preserved. A drawback of the adaptive methods is that they usually lead to implicit methods even if the original method is explicit.

A technique to overcome this difficulty was developed by Huang and Leimkuhler, [13], for the construction of time-reversible explicit Störmer-Verlet integrators with a variable stepsize. This approach is based on the introduction of a time reparametrization similar to the Sundman transformation used in celestial mechanics:

$$\tau \mapsto t(\tau), \quad t' = g(q), \tag{18}$$

where the derivative with respect to fictive time τ is denoted by a prime, and $g: \mathcal{M} \to \mathbb{R}^+$ is a smooth function. Then, a differential equation $\dot{\boldsymbol{q}} = X(\boldsymbol{q})$ will be transformed in

$$\boldsymbol{q}' = g(\boldsymbol{q})X(\boldsymbol{q}), \quad t' = g(\boldsymbol{q}). \tag{19}$$

After this transformation, Eq. (19) is integrated using a method with a constant stepsize $\varepsilon := \tau_n - \tau_{n-1}$.

Following [13,14] an adaptive Zhang-Qin method for the point vortex dynamics may be constructed introducing a variable in problem (5)–(18):

$$\gamma := g(\boldsymbol{q}). \tag{20}$$

Let us consider the discretization for (5)–(18) given by the map $\Xi_\varepsilon: (q_n, \gamma_n) \mapsto (q_{n+1}, \gamma_{n+1})$ defined as follows:

$$q_{n+(1/2)} = \phi_{(1/2)\varepsilon\gamma_n}(q_n),$$

$$\gamma_{n+1} = -\gamma_n + 2g(q_{n+(1/2)}),$$

$$q_{n+1} = \phi^*_{(1/2)\varepsilon\gamma_{n+1}}(q_{n+(1/2)}), \tag{21}$$

where $\phi_{\varepsilon\gamma_n/2}$ is the integrator defined in (13), with $h = \varepsilon\gamma_n/2$. Initial conditions for (21) are: $q_0 = \boldsymbol{q}(0)$ and $\gamma_0 = g(q_0)$. Once the numerical solution of (5)–(18) is determined, the real time variable t can be derived by means of the trapezoidal rule applied to $(18)_2$:

$$t_{n+1} = t_n + (1/2)(g(q_{n+1}) + g(q_n))\varepsilon. \tag{22}$$

If the scaling function (20) is chosen satisfying the condition

$$g(\rho(q)) = g(q), \tag{23}$$

then the method Ξ_ε established (21) is time reversible under involution

$$\rho(q, \gamma) \mapsto (\bar{q}, \gamma). \tag{24}$$

A natural choice for $g(q)$ satisfying (23) is given by the Euclidean norm of the vector field $X(\boldsymbol{q})$,

$$g(q) := \|X(q)\|, \tag{25}$$

so that the parameter τ may be interpreted as the arc length of the trajectory.

On the other hand, the inverse mapping $\Xi_\varepsilon^{-1}: (q_{n+1}, \gamma_{n+1}) \mapsto (q_n, \gamma_n)$ is

$$q_{n+(1/2)} = (\phi_{(1/2)\varepsilon\gamma_{n+1}})^{-1}(q_{n+1}),$$

$$\gamma_n = -\gamma_{n+1} + 2g(q_{n+(1/2)}),$$

$$q_n = (\phi_{(1/2)\varepsilon\gamma_n})^{-1}(q_{n+(1/2)}), \tag{26}$$

which, due to $(\phi^*_m)^{-1} = \phi_{-m}$, coincides with $\Xi_{-\varepsilon}$. Therefore, the method Ξ_ε is time symmetric and consequently it is of even order (in particular, second order since ϕ is a first order method).

By applying Yoshida's composition technique [23] one may derive higher order methods based on the map Ξ_ε defined in (21). In this paper we consider, for a given split of the Hamiltonian vector field, the five-stage fourth order method due to Suzuki, obtained by the symmetric composition of symmetric methods with coefficients:

$$c_1 = c_2 = c_4 = c_5 = (4 - 4^{1/3})^{-1}, \quad c_3 := 1 - 2c_1$$

(see [30] for other good methods for arbitrary splits). The resulting method, referred from now on as ZQ4A, is given by:

$$\Psi_\varepsilon := \Xi_{c_5\varepsilon} \circ \Xi_{c_4\varepsilon} \circ \Xi_{c_3\varepsilon} \circ \Xi_{c_2\varepsilon} \circ \Xi_{c_1\varepsilon}, \tag{27}$$

which retains the properties of time symmetry and ρ reversibility.

IV. EXCHANGE-SCATTERING OF A VORTEX PAIR

On this section we apply, in the first place, the ZQ4A method to a three-vortex system with strengths of the form $\kappa_1 = \kappa_2 = -\kappa_3 > 0$. For this model both the scattering of a vor-

tex pair (V_1,V_3) and the exchange of a vortex pair (V_1 and V_2) may occur. These phenomena were studied by Aref [18] and are present, for example, in Atmospheric Physics (see [24]). Also an application of the ZQ4A method is made to a vortex system in which a small vortex is added to the above model.

A. Choice of the initial values

For the three-point vortex problem there exists (see [18,25]) a classification of all possible trajectories, given the strengths of the vortices. This classification is made attending to the linear stability of the critical points of the vector field which appears in the differential equation for the evolution of the triangular configuration of three vortices expressed in trilinear coordinates. This classification leads to several phase diagrams which contain information about the relative motion of the vortices, but not about the absolute motion.

From the classification in [18,25] one concludes that for a vortex system with $\kappa_1=\kappa_2=-\kappa_3>0$ both phenomena exchange and scattering of a vortex pair are present if the strengths of the vortices satisfy the following conditions:

$$\kappa_1\kappa_2+\kappa_2\kappa_3+\kappa_3\kappa_1<0, \quad \kappa_2+\kappa_3=0, \tag{28}$$

and convenient initial values are considered. This model corresponds to the exceptional cases II-1 and II-2 in the classification of Tavantzis and Ting [25]. Using the notation R_1,R_2,R_3 to denote the distances between the pairs of vortices (V_2,V_3), (V_1,V_3), and (V_1,V_2), the trilinear coordinates are defined

$$x_i := \frac{R_i}{R_1+R_2+R_3}, \quad i=1,2,3, \tag{29}$$

satisfying the condition $x_1+x_2+x_3=1$. Let us choose as initial configuration a point in the region of the phase space determined by the inequalities

$$x_3>x_1, \quad x_3>x_2, \quad 8x_1^2x_2^2>x_3^2(x_3^2-x_2^2-x_1^2). \tag{30}$$

Points satisfying (30) are in a region of the phase space (see region 6 in Fig. 8 of Ref. [25]) in which the trajectories are aperiodic.

The exchange of the vortices V_1 and V_2 occurs at an instant t^* when the relative distances between vortices satisfy $R_1=R_2$. Denoting by $P_1^*=(q_1^*,q_4^*)$, $P_2^*=(q_2^*,q_5^*)$, $P_3^*=(q_3^*,q_6^*)$ the position of the vortices at time t^*, we choose the initial configuration as follows:

$$\boldsymbol{q}_0=(q_1^*,q_2^*,q_3^*,q_4^*,q_5^*,q_6^*). \tag{31}$$

Note that for each point of the phase space with trilinear coordinates (x_1,x_2,x_3) satisfying (30), if this point is on the trajectory, then the point (x_2,x_1,x_3) also lies on the same trajectory.

B. Symmetry of the exact orbit

Given a vector field X with flow ϕ_t, reversible under an involution σ, and an initial configuration $\boldsymbol{q}_0$, the orbit of $\boldsymbol{q}_0$ is defined

$$\mathrm{Orb}(\boldsymbol{q}_0) := \{\boldsymbol{q} \,|\, \phi_t(\boldsymbol{q}_0)=\boldsymbol{q}, \quad t\in\mathbb{R}\}. \tag{32}$$

The orbit $\mathrm{Orb}(\boldsymbol{q}_0)$ is called *symmetric* if it is invariant under σ:

$$\sigma(\mathrm{Orb}(q_0))=\mathrm{Orb}(q_0). \tag{33}$$

In particular, for the vector field (5) and the initial condition $\boldsymbol{q}_0$ chosen in (31), the orbit $\mathrm{Orb}(\boldsymbol{q}_0)$ is symmetric with respect to the axis determined by the vector

$$\boldsymbol{u} := \overrightarrow{P_1^*P_3^*}-\overrightarrow{P_2^*P_3^*}. \tag{34}$$

We take as Ox axis the line through P_3^* directed along $\boldsymbol{u}$, and the Oy axis along the line $P_1^*P_2^*$.

Let $\varrho:\mathbb{R}^6\to\mathbb{R}^6$ be the linear reflection with respect to the subspace

$$\mathcal{E} := \{(q_1,q_2,q_3,0,0,0) \,|\, q_1,q_2,q_3\in\mathbb{R}\} \tag{35}$$

defined

$$\varrho:(q_1,q_2,q_3,q_4,q_5,q_6)\mapsto(q_1,q_2,q_3,-q_4,-q_5,-q_6), \tag{36}$$

and $\iota:\mathbb{R}^6\to\mathbb{R}^6$ the linear mapping exchanging the vortices V_1 and V_2:

$$\iota:(q_1,q_2,q_3,q_4,q_5,q_6)\mapsto(q_2,q_1,q_3,q_5,q_4,q_6). \tag{37}$$

From the involutions ϱ and ι one may build an involution

$$\sigma := \varrho\circ\iota, \tag{38}$$

under which the vector field (5) is also reversible.

A well known result [26] establishes that, for σ-reversible vector fields, condition (33) for a symmetric orbit is equivalent to the existence of a point in the orbit which remains fixed under the involution σ. The action of the map (38) on $\mathbb{R}^6$ leaves the tridimensional subspace

$$\mathrm{Fix}(\sigma) := \{(a,a,b,c,-c,0) \,|\, \forall \quad a,b,c\in\mathbb{R}\}, \tag{39}$$

fixed. Therefore, since the initial value $\boldsymbol{q}_0$ chosen in (31) is a point in $\mathrm{Fix}(\sigma)$, orbit $\mathrm{Orb}(\boldsymbol{q}_0)$ is symmetric with respect to $\mathcal{E}$.

Observe that Synge's theorem [27] yields a sufficient condition for reflection symmetry based on the existence of collinear configurations. This condition is not applicable in the exchange-scattering phenomenon since there exist no collinear configurations in region (30). Even so, the orbit $\mathrm{Orb}(\boldsymbol{q}_0)$ is symmetric with respect to σ. Moreover, if there exists a nonsymmetric first integral I (i.e., such that $I(\sigma(\boldsymbol{q}))\neq(I(\boldsymbol{q}))$) then only orbits crossing the set $\mathcal{F}(I)=\{\boldsymbol{q} \,|\, I(\boldsymbol{q})=I(\sigma(\boldsymbol{q}))\}$ may be symmetric (cf. [28]). For the motion of point vortices the first integral Y in (2) is not σ symmetric and the relation $Y(\boldsymbol{q})=Y(\sigma(\boldsymbol{q}))$ is verified, so such necessary condition of symmetry is satisfied.

C. Numerical experiment

In order to increase the efficiency of a method for the numerical integration of the exchange-scattering model it is useful to apply a time stepping which allows one to employ large stepsizes when the distance from the pair (V_1,V_3) [or

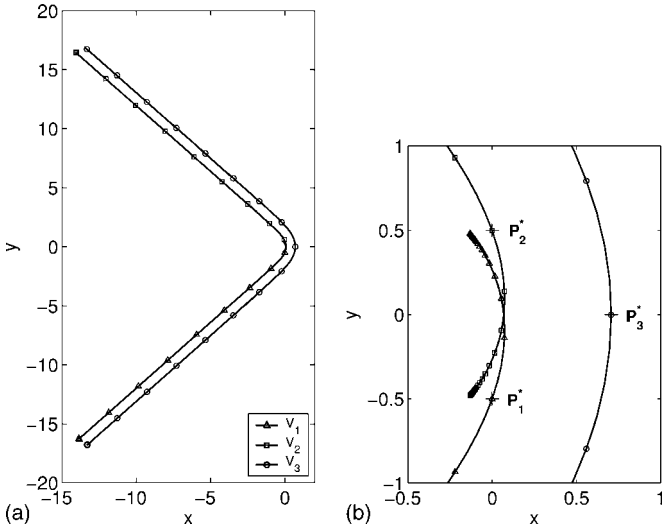

FIG. 1. (a) Trajectories of three vortices V_1, V_2, V_3 with exchange-scattering of a vortex pair. (b) Close-up of the trajectories about (0, 0). Points P_1^*, P_2^*, P_3^* indicate the position in which the exchange takes place.

(V_2, V_3) after the vortex exchange] to the vortex V_2 (respectively, V_1) is great. Here we take for the strengths of the vortices the values $\kappa_1=\kappa_2=-\kappa_3=1$, and assume that initially the vortices are located in the points: $P_1^*=(0,-\frac{1}{2})$, $P_2^*=(0,\frac{1}{2})$, and $P_3^*=(\frac{\sqrt{2}}{2},0)$, so that the point

$$\boldsymbol{q}_0^* = \left(0,0,\frac{\sqrt{2}}{2},-\frac{1}{2},\frac{1}{2},0\right) \tag{40}$$

is in region (30) of the phase space.

Applying the fourth order Zhang-Qin method (hereafter referred to as ZQ4) with constant stepsize $h=-0.05$, integration backward in time of (5) from the initial value (40) gives at the time $t=-100$ the point

$$\boldsymbol{q}_I = (-13.86,-0.13,-13.29,-16.29,-0.48,-16.77). \tag{41}$$

In a similar way, now with positive stepsize $h=0.05$, one obtains at $t=200$ a point $\boldsymbol{q}_F$ such that $\|\sigma(\boldsymbol{q}_F)-\boldsymbol{q}_I\|=1.7\times10^{-7}$, which reflects the symmetry of the orbit for the three-vortex system. On an Athlon XP 2600+2.08 GHz processor the CPU time spent is of 1.2 s. For the same problem, the MATLAB code ODE45, based on the Dormand-Prince (4, 5) pair, with tolerance Tol$=10^{-9}$ (for which the maximum deviation of the energy is of the same order to that given by ZQ4), the CPU time required is 0.1 s. In Fig. 1 it is shown the trajectories of the vortices for $-100\leqslant t\leqslant 100$.

1. Scaling functions

The performance of the adaptive method ZQ4A depends on the scaling function chosen in (18), so it is necessary to apply some criterion to select a suitable scaling function for each model under consideration. For classical Hamiltonian systems (of the form kinetic plus potential energy) such a criterion is based on the invariance of the main part of the potential in regions where the mechanical system evolves fast.

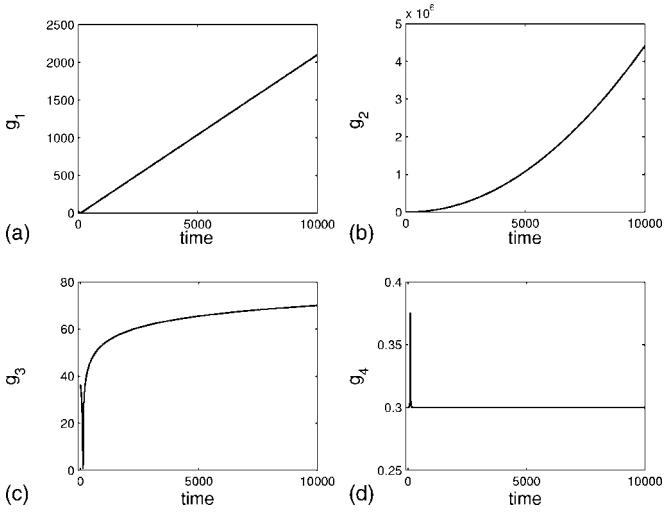

FIG. 2. Scaling function as time functions. Functions g_1, g_2, g_3, g_4 correspond to (42) (with $\alpha=\frac{1}{2}$), (43)–(45), respectively.

However, for point-vortex systems the Hamiltonian is not split in kinetic and potential energy thus the choice of the scaling function must be based on other properties in each particular model. Therefore, for the exchange-scattering model described above, from the symmetry properties of the vortex orbits one may build useful scaling functions using powers of the distance from the vortex V_3 to the center of vorticity

$$g(\boldsymbol{q}) = ((q_1+q_2-2q_3)^2+(q_4+q_5-2q_6)^2)^{\alpha}. \tag{42}$$

Also, from both properties of preservation of the angular momentum and energy and the qualitative properties of the orbit shown in Fig. 1, useful scaling functions may be defined

$$g(\boldsymbol{q}) = |\kappa_1|(q_1^2+q_4^2)+|\kappa_2|(q_2^2+q_5^2), \tag{43}$$

related to the angular momenta of the vortices V_1 and V_2, or the function

$$g(\boldsymbol{q}) = -\frac{10^3}{8\pi}(\kappa_1\kappa_3\ln[(q_1-q_3)^2+(q_4-q_6)^2] + \kappa_2\kappa_3\ln[(q_2-q_3)^2+(q_5-q_6)^2]), \tag{44}$$

proportional to the energy of V_1 and V_2.

The behavior of the expressions (42)–(44) as time functions for the exchange-scattering model is shown in Fig. 2 where it is observed that for each $\boldsymbol{q}(t)$, these scalar-valued functions are positive and they increase from a time.

In addition to the scaling functions built from properties of the motion known in advance, a popular choice consists in

$$g(q) = \|X(q)\|, \tag{45}$$

for which the reparametrization (18) in terms of the Euclidean norm of the vector field (5) normalizes the vector field and may be interpreted as a control of the arc-length measured along the orbit in the unit time. Furthermore, the pa-

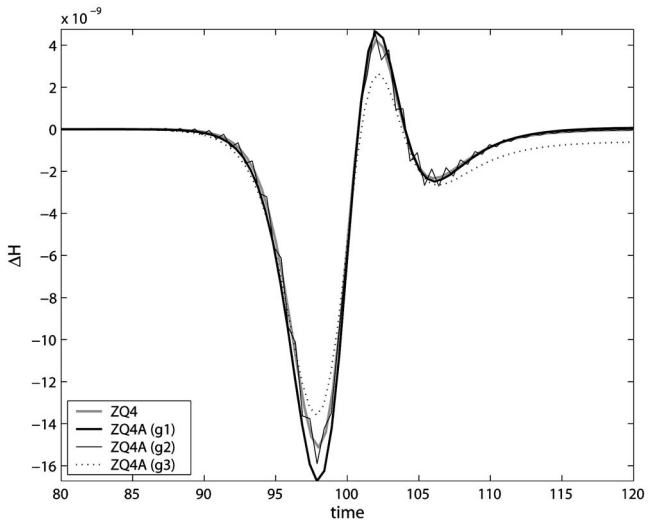

FIG. 3. Energy error in a vicinity of $t=100$ for the solutions obtained by using the methods ZQ4 and ZQ4A with scaling function g_1, g_2, and g_3 (see caption of Fig. 2). The real stepsize, h, and the stepsize of virtual time, ε, has been adjusted so that the maximum energy error be similar in all cases ($h=0.5$; $\varepsilon=0.01$ for g_1, and $\varepsilon=0.001$ for g_2 and g_3).

rametrization given by the function (45) has the property that the numerical approximations $\boldsymbol{q}_n$ in the phase space are almost equidistant. However, a drawback of this scaling function is that it requires us to compute the vector field X in each step, something which might be very expensive. For the model we are considering, the behavior of the función (45) is shown in Fig. 2(d) where we see that this function is almost constant (after a small time interval), so that for the exchange-scattering problem this scaling function becomes useless.

Once a scaling function g is chosen, it is necessary to restrict the stepsize Δt to an interval $\Delta t_m \leqslant \Delta t \leqslant \Delta t_M$ to avoid very large or small values of Δt. For this, instead of $g(\boldsymbol{q})$ one may apply the regularized function (cf. [14]):

$$\hat{g}(\boldsymbol{q}) = M\frac{g(\boldsymbol{q})+m}{g(\boldsymbol{q})+M}, \tag{46}$$

where $M := \Delta t_M/\varepsilon$ and $m := \Delta t_m/\varepsilon$.

To compare the solutions obtained by means of ZQ4A with the scaling functions (42)–(44) we integrate (5) with the initial value (41) in the interval $0 \leqslant t \leqslant 200$, using the split $X = X_{H_{23}} + X_{H_{12}} + X_{H_{13}}$. The energy error as a time function for each of these functions is shown in Fig. 3 where the stepsizes have been adjusted so that the maximum error be similar in all cases: $\varepsilon=0.01$ for (42) and $\varepsilon=0.001$ if (43) or (44) are used. The behavior of the energy error is similar for each of these cases. In Fig. 3 the energy error for the solution given by the fixed stepsize method ZQ4 with $h=0.5$ has also been drawn. After the instant in which the exchange of vortices takes place, all simulations return a value of ΔH approximately equal to zero. In the first lines in Table I the final differences $\Delta H(200)$ are shown. The best results obtained with ZQ4A are given by using the scaling function (43).

2. Comparison of different splitting algorithms

To implement the ZQ4A method, apart from the choice of a scaling function, one must also choose one of the six possible splits of the Hamiltonian vector field.

For a point vortex model (4), with $N=3$, the Hamiltonian function H may be decomposed as a sum of three functions H_a, H_b, and H_c, associated with the vortex pairs (V_1, V_2), (V_1, V_3), and (V_2, V_3), respectively. Each of the corresponding Hamiltonian systems are integrable and the solution may be efficiently programmed. By means of the composition (14) the elementary integrators $\varphi^{[a]}$, $\varphi^{[b]}$, and $\varphi^{[c]}$, associated with H_a, H_b, and H_c, respectively, one obtains the scheme

$$\Phi_h^{[i,j,k]} = \varphi_{h/2}^{[k]} \circ \varphi_{h/2}^{[j]} \circ \varphi_h^{[i]} \circ \varphi_{h/2}^{[j]} \circ \varphi_{h/2}^{[k]}, \tag{47}$$

where $[i,j,k]$ is an arbitrary permutation of $[a,b,c]$. (From now on we use the symbol $[i,j,k]$ to make reference to a particular splitting.)

TABLE I. Comparison of various integrators applied to the exchange-scattering model. $\Delta H(200)$ measures the energy error for each method at the time $t=200$. $\|\Delta \boldsymbol{q}(0)\|$ measures the separation between the point $\boldsymbol{q}_0$ and the point obtained by integrating backward from $q(200)$ with opposite stepsize. The last two rows show the maximun energy error and the CPU-time employed by the different methods for the stepsizes selected in a long time interval $[0, 10^4]$. (The results recorded have been computed using the splitting $[c,a,b]$.)

	ZQ4	ZQ4A	ZQ4AP	ZQ4AS1	ZQ4AS2
$\Delta\lvert H(200)\rvert^{a}$	5.9×10^{-15}	1.0×10^{-10}	7.9×10^{-15}	2.1×10^{-15}	1.7×10^{-15}
$\Delta\lvert H(200)\rvert^{b}$	1.9×10^{-13}	5.5×10^{-10}	9.2×10^{-15}	1.9×10^{-11}	2.5×10^{-12}
$\Delta\lvert H(200)\rvert^{c}$	6.0×10^{-16}	3.8×10^{-11}	2.6×10^{-14}	2.0×10^{-11}	3.4×10^{-12}
$\|\Delta \boldsymbol{q}(0)\|^{a}$	9.0×10^{-10}	4.4×10^{-12}	1.0×10^{-6}	2.6×10^{-5}	1.5×10^{-6}
$\|\Delta \boldsymbol{q}(0)\|^{b}$	7.2×10^{-10}	2.4×10^{-9}	2.0×10^{-6}	2.6×10^{-5}	1.6×10^{-6}
$\|\Delta \boldsymbol{q}(0)\|^{c}$	2.6×10^{-10}	5.7×10^{-9}	6.8×10^{-8}	2.6×10^{-5}	1.4×10^{-6}
$\lvert\Delta H\rvert_{\max}^{a}$ $(t\in[0,10^4])$	1.5×10^{-8}	1.7×10^{-8}	5.4×10^{-9}	1.5×10^{-8}	1.5×10^{-8}
CPU time	21	4.6	9	11	11

[a]Splitting $[c,a,b]$.
[b]Splitting $[a,c,b]$.
[c]Splitting $[b,c,a]$.

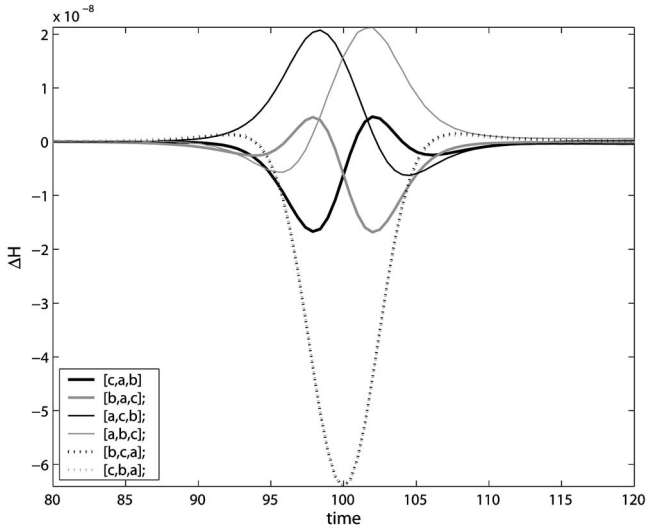

FIG. 4. Energy error for the solutions obtained with method ZQ4A using different Hamiltonian splittings. The scaling factor $g=d(V_3,C)$ and the stepsize $\varepsilon=0.01$ has been employed.

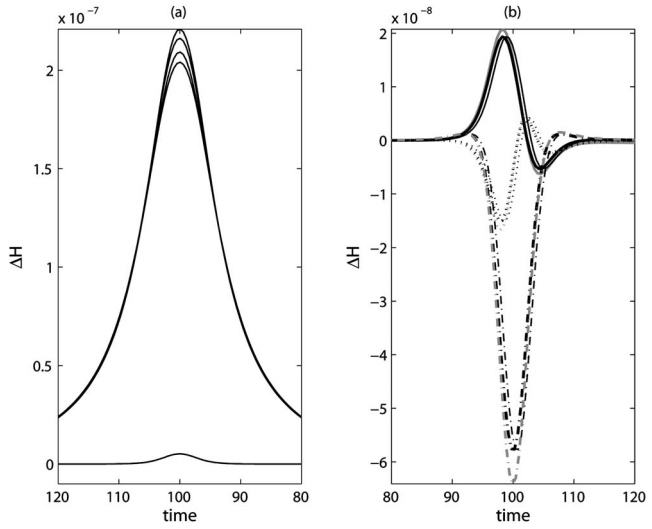

FIG. 5. (a) Evolution of ΔH for the solution of the exchange-scattering model obtained using the adaptive method with the Scovel projection, for different splittings. (b) Evolution of ΔH for the solutions given by ZQ4AS1 (dark-thick lines) and ZQ4AS2 (dark-thin lines) compared with the solution obtained applying ZQ4 (gray lines). Solid lines correspond to splitting $[a,b,c]$, dash-dotted lines to $[c,a,b]$, and dotted lines to $[b,c,a]$.

Now, using the initial value (41) and a time interval of length $T=200$ we will study the behavior of the energy evolution for the solution given by ZQ4A for each of the possible Hamiltonian splits. In Fig. 4 one observes a property also present in the solution given by ZQ4, namely, there exist pairs of solutions

$$\Phi^{[a,i,j]}(\boldsymbol{q}_0), \quad \Phi^{[i,a,j]}(\boldsymbol{q}_0), \Phi^{[i,j,a]}(\boldsymbol{q}_0), \tag{48}$$

such that the corresponding energy errors as functions of time are mirror symmetric about the line $t=100$. Also, Fig. 4 shows that after the exchange of vortices (at $t=100$) all solutions return approximately the initial value $\Delta H(0)$, although only those corresponding to the splits $[a,b,c]$ and $[a,c,b]$ are almost overlapped. In Appendix B a backward error analysis is given to justify these properties of the numerical solutions.

In Table I it is observed that the ZQ4 method gives a solution for which the final energy drift is smaller than that in ZQ4A. This suggests that a switch between both methods in a region near $t=100$ may retain the properties of recovering the initial energy present in ZQ4 and the efficiency of the adaptive method.

For this we divide the interval of integration in two parts: the first one far from the point in which the exchange of vortices takes place (say $|q_6|>10$), and the other one near this point $|q_6|\leqslant 10$). In the first region the ZQ4A method is applied using a determined scaling function [e.g., (42) with $\alpha=\frac{1}{2}$] and in the second region one integrates using ZQ4A with $g(\boldsymbol{q})=0$ (fixed stepsize method). The resulting integrator (denoted by ZQ4AS1) gives a decrease of the energy drift, see Table I.

The scheme ZQ4AS1 uses a discontinuous scaling function. An analogous construction, applying in this case the switching technique by Kværnø and Leimkuhler [32], may be carried out by defining a suitable smooth function ς which goes from zero to one in a finite interval. The vector field X is decomposed in two parts $X_1=X(\varsigma(q))$ and $X_2:=X(1-\varsigma(q))$. Denoting by $\Phi^{[1]}$ the integrator ZQ4A with scaling function (42) and by $\Phi^{[2]}$ the integrator with fixed stepsize, a method may be obtained by composition:

$$\Phi^{[1]}_{(1-\varsigma)h} \circ \Phi^{[2]}_{\varsigma h}. \tag{49}$$

Because of the symmetry of the trajectory $(q_3(t),q_6(t))$ of vortex V_3 with respect to the coordinate axis Oy, we use the piecewise smooth function

$$\varsigma(\boldsymbol{q}) := \begin{cases} 0 & \text{if } 0 \leqslant |q_6| < 10, \\ 100(203-20|q_6|)(|q_6|-10)^2 & \text{if } 10 \leqslant |q_6| < 10.1, \\ 1 & \text{if } |q_6| \geqslant 10.1, \end{cases} \tag{50}$$

which is nonnegative and symmetric with respect to $q_6=0$. Let us denote by ZQ4AS2 the integrator (49).

The energy error for the numerical solutions given by ZQ4AS1 and ZQ4AS2 are shown in Fig. 5(b), both solutions are similar except for a small time shift. One might remark that if the transition interval in the function $\varsigma(q_6)$ in (50) is enlarged, then the energy drift increases.

D. Symmetry of the numerical orbit

In the study of the symmetry of the exact orbit in Sec. IV C, we saw that by using the involution σ, under which the vector field X is time reversible, a simplification of this study is obtained. However, given a splitting of the Hamiltonian, for example

$$H = H_{12} + H_{13} + H_{23} =: H_a + H_b + H_c, \tag{51}$$

the vector fields $X_a = \mathbb{B}\,\mathrm{grad}\,H_a$ are not σ-reversible but satisfy the relation

$$\sigma \circ (X_a, X_b, X_c) \circ \sigma = -(X_a, X_b, X_c) \tag{52}$$

which reflects the vortex exchange phenomenon. The partial methods $\varphi_h^{[a]}$, (A1), in the Zhang-Qin method (13) corresponding to the vector fields X_a satisfy

$$\sigma \circ (\varphi_h^{[a]}, \varphi_h^{[b]}, \varphi_h^{[c]}) \circ \sigma = (\varphi_{-h}^{[a]}, \varphi_{-h}^{[c]}, \varphi_{-h}^{[b]}). \tag{53}$$

Only the method $\varphi_h^{[a]}$ is σ-reversible. Consequently the composition (13) (with $\nu=3$)

$$\phi_h := \varphi_h^{[a]} \circ \varphi_h^{[b]} \circ \varphi_h^{[c]} \tag{54}$$

is not σ-reversible. One obtains

$$\sigma \circ \phi_h \circ \sigma := \varphi_{-h}^{[1]} \circ \varphi_{-h}^{[3]} \circ \varphi_{-h}^{[2]} =: \tilde{\phi}_{-h} \neq \phi_h^{-1}, \tag{55}$$

where $\tilde{\phi}_h$ is the method associated with the splitting $[a,b,c]$.

Given a map Φ, let us denote by $\mathrm{orb}(\boldsymbol{q}_0)$ the discrete orbit associated to a map Φ:

$$\mathrm{orb}(\boldsymbol{q}_0) := \{\boldsymbol{q} | q = \Phi^n(\boldsymbol{q}_0), n \in \mathbb{Z}\}. \tag{56}$$

If Φ has an involutory reversing symmetry R, the orbit $\mathrm{orb}(\boldsymbol{q}_0)$ is symmetric if and only if (cf. Ref. [26])

$$\mathrm{orb}(q_0) \cap [\mathrm{Fix}(R) \cup \mathrm{Fix}(R \circ \Phi)] = \emptyset. \tag{57}$$

In particular, for the ϱ-reversible flow map Ψ_ε in (27) given by the ZQ4A method and the point q_0^* (40) it turns out that $q_0^* \notin \mathrm{Fix}(\varrho) \cup \mathrm{Fix}(\varrho \circ \psi_\varepsilon)$, so that the discrete orbit $\mathrm{orb}(\boldsymbol{q}_0^*)$ is not symmetric under reflections on the subspace (35). On the other hand, if one considers the involution σ, instead of ϱ, we have that, although there exists a point such that $\boldsymbol{q}_0^* \in .\mathrm{Fix}(\sigma)$, however, the map Ψ_ε is not σ reversible. Therefore, condition (57) is not applicable to study the symmetry of the orbit given by the ZQ4A method.

Even so, one may obtain a σ-reversible method, to which it is applicable the theorem on symmetric orbits, using the Scovel projection (see [29]) applied to the mapping: Ψ_ε

$$\bar{\Psi}_\varepsilon := \Psi_{/2} \circ \sigma \circ \Psi_{\varepsilon/2}^{-1} \circ \sigma. \tag{58}$$

Then, $\mathrm{orb}(\boldsymbol{q}_0)$, with $\boldsymbol{q}_0$ given in (41), satisfies the symmetry condition (57) under the map $\bar{\Psi}_\varepsilon$ defined in (58). In general, the projected method associated with (58) is not time symmetric. However, as reversibility is a property related to more basic properties of dynamics than the time reversibility [29], it is useful to apply the projection technique to a high-order method to construct a reversible method. The abbreviation ZQ4AP will be used to make reference to the projected method associated with ZQ4A. We showed in Fig. 5 the behavior of the energy error, for all possible Hamiltonian splittings, corresponding to the solutions obtained by means of ZQ4AP. No drift is observed for H (see Table I). In addition, one observes that the evolution of the energy error $\Delta H(t) := H(t) - H(0)$ is symmetrical with respect to $t=100$, in contrast to the behavior shown for the evolution $\Delta H(t)$ given by ZQ4A (gray curves in Fig. 5).

An estimation of the lack of time-symmetry of the solution given by ZQ4AP may be evaluated integrating, in the first place, forward in time taking a time interval $0 \leqslant t \leqslant 200$, a fictitious time step $\varepsilon = 0.1$ and an initial value (41), to obtain the point $q(200)$, and next integrating backward in time with $\varepsilon = -0.1$ and initial value $q(200)$ to obtain the point $\bar{q}$ at $t=200$. The distance between q_0 and $\bar{q}$ is

$$\|q_0 - q_0'\| = 10^{-6}, \tag{59}$$

for the splitting $[c,a,b]$. In contrast, following the same program but now using the t-symmetric method ZQ4A, one obtains a point $\bar{q}'$ such that

$$\|q_0 - \bar{q}_0'\| = 4.4 \times 10^{-12}. \tag{60}$$

Table I shows the shifts $\|q_0 - \bar{q}_0'\|$ for various methods and different splittings for stepsizes which give analogous results for the maximum energy error. Methods ZQ4 and ZQ4A give good results in this test of reversibility (in particular for the adaptive method with the splitting $[c,a,b]$. For methods ZQ4AS1 and ZQ4AS2 the reversibility of the solution is not so good.

V. LONG-TERM INTEGRATION BY USING THE METHOD ZQ4A

In this section we explore the properties of preservation of the first integrals and compare the efficiency of the schemes ZQ4 and ZQ4A when applied to the following simple three vortex models: (1) The exchange-scattering model studied above; (2) A self-similar expansion of three vortices, and (3) a vortex system moving in a bounded region on the plane.

A. The exchange-scattering model

For this model we have studied the evolution of the energy integral about the time $t=100$ in which the deviation of the energy is maximal (see Fig. 4). Far from this region the energy remains approximately constant. Now, we study the evolution of the other first integrals. Figure 6 shows the behavior of the conserved quantities related to the linear and angular momentum of the vortex system described in Sec. IV C, when this model is integrated over a long interval of $t \in [0, 10^4]$ using the numerical methods discussed above. In Fig. 6(a) we plot the deviation of the invariant X^2+Y^2 associated with the linear impulse as a function of time. All the methods applied present a similar evolution, ZQ4A being the method with the smallest error.

Figure 6(b) shows the evolution of the angular momentum error. Again it is ZQ4A the method with a better behavior, the larger error being obtained with ZQ4, which displays a sudden change for $t \approx 6000$.

To compare the efficiency of ZQ4 and ZQ4A (and the variants of the adaptive method studied in Sec. IV D) we consider a particular splitting, $[a,b,c]$, and plot the maximun energy error against the CPU-time employed by each method for integration over the interval $t \in [0, 10^4]$. Figure 7(a) shows that ZQ4A is the most efficient method, one may also observe that Scovel's projection and the switching technique give rise to a loss of efficiency although they always remain

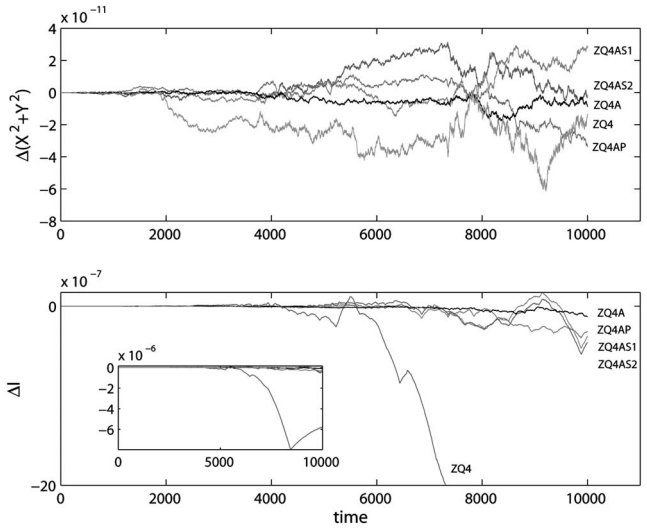

FIG. 6. (a) Evolution of the first integral $|X+iY|^2$ in the exchange-scattering model solved using the Zhang-Qin method and the adaptive method ZQ4A and different variants of this method. (b) *Idem* for the error in the angular momentum.

more efficient than the fixed stepsize method.

B. Self-similar expansion

Now let us consider three vortices with intensities $\kappa_1 := -5$, $\kappa_2 = -4$, $\kappa_3 = 20/9$, such that the harmonic mean

$$\eta := \tfrac{1}{3}(\kappa_1^{-1} + \kappa_2^{-1} + \kappa_3^{-1}), \tag{61}$$

is vanished. The initial configuration is chosen so that the vortices expand self-similarly. An initial configuration of this class may be determined following Ref. [18]. Let us choose the Ox axis along the line determined by the vortices V_1, V_2 in $t=0$, the origin O being the center of vorticity for the pair V_1, V_2. In these coordinates the initial positions are situated in the points

$$V_1 := \left(-\tfrac{4}{9}, 0\right), \quad V_2 = \left(\tfrac{5}{9}, 0\right), \quad V_3 = (X, Y), \tag{62}$$

where

$$X := \tfrac{1}{2}(x_1 + x_2), \quad Y := \sqrt{r^2 - X^2}, \tag{63}$$

and

$$r = l_{12}\sqrt{\frac{\kappa_1 + \kappa_2 + \kappa_3}{\kappa_1 + \kappa_2}}, \tag{64}$$

is the radius of the circumference formed by the points in the plane satisfying the condition

$$\tfrac{1}{3}(\kappa_3^{-1} l_{12}^2 + \kappa_1^{-1} l_{23}^2 + \kappa_2^{-1} l_{31}^2) = 0, \tag{65}$$

where l_{ij} are the intervortical separations. The third vortex V_3 has been placed on the segment P_1, P_2 on the circumference shown in Fig. 8 in [18], so each vortex moves away from the center of vorticity

$$C := (-0.021, -0.284) \tag{66}$$

following logarithmic spirals [see Fig. 8(a)].

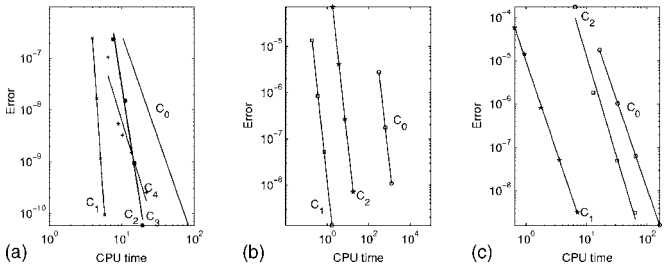

FIG. 7. Comparison of the efficiency of various methods applied to different models. In the three figures the curve C_0 corresponds to the efficiency of the ZQ4 method. (a) Exchange-scattering model: curves C_i, $i=1,2,3,4$, correspond to ZQ4A, ZQ4AP, ZQ4AS1, and ZQ4AS2, respectively. (Curves C_2 and C_3 appear overlapped.) (b) Self-similar expansion: C_1 and C_2 correspond to the solution given by ZQ4A with scaling factors $d(V_3, C)$ and $\|X_H\|^{-1}$, respectively. (c) Bounded motion model: C_1 and C_2 correspond to the solutions given by ZQ4A using the scaling functions $d(V_1, C)^{3/2}$ and $\|(\dot{q}_3, \dot{q}_6)\|^{-1}$, respectively.

The numerical solution corresponding to this initial configuration has been obtained applying the ZQ4A method over a time interval $t \in [0, 10^4]$ using the scaling function $g(\boldsymbol{q}) = \|(\dot{q}_3, \dot{q}_6)\|^{-1}$, related to the velocity of the V_3 vortex, and the function (42) with $\alpha = \frac{1}{2}$. In Fig. 8(a) the stepsize of real time is plotted as a function of time. In Figs. 8(c) and 8(d) the evolution of the error in the first integrals is shown. One observes that the absolute value of $X+iY$ and the angular momentum show errors increasing with time. However, the energy remains almost constant after a short time interval in which the energy error oscillates fast.

Each instantaneous configuration in the evolution of this vortex system may be considered as the initial configuration of the vortex system with intensities $-\kappa_1$, $-\kappa_2$, and $-\kappa_3$ whose evolution leads to a collapse in the center of vorticity. It is well known that a necessary condition for the self-similar collapse (see, e.g., [19]) consists in the vanishing of the invariant

$$M := 2(-\kappa_1 - \kappa_2 - \kappa_3)I - Q^2 - P^2, \tag{67}$$

made up from the first integrals of the system. Therefore, the error ΔM may be taken as a measurement of the accuracy of the numerical solutions. In Fig. 8(c) it is shown that ΔM is fast decreasing.

In the self-similar motion the ratios $\rho := l_{\alpha\beta}/l_{\alpha'\beta'}$ of the vortex separations must remain constant along the expansion. In Fig. 8(f) we have plotted the deviation of ρ from its initial value. One observes that, after an initial oscillatory phase, the function $\rho(t)$ remains constant, the graphs of ΔH and $\Delta\rho$ being analogous.

The comparison of the efficiency of the ZQ4A method, using the scaling functions $g(\boldsymbol{q}) = \|(\dot{q}_3, \dot{q}_6)\|^{-1}$ and (42), with $\alpha = \frac{1}{2}$, and the ZQ4 method is established in Fig. 7(b), where one sees that the selection of a suitable scaling function [(42) in this case] may improve the performance of the method.

C. Motion in a bounded region

The two models discussed above evolve in an unbounded region of the plane. Now, we consider three vortices whose intensities $\kappa_1 = -5$, $\kappa_2 = -4$, and $\kappa_3 = 5$ satisfy

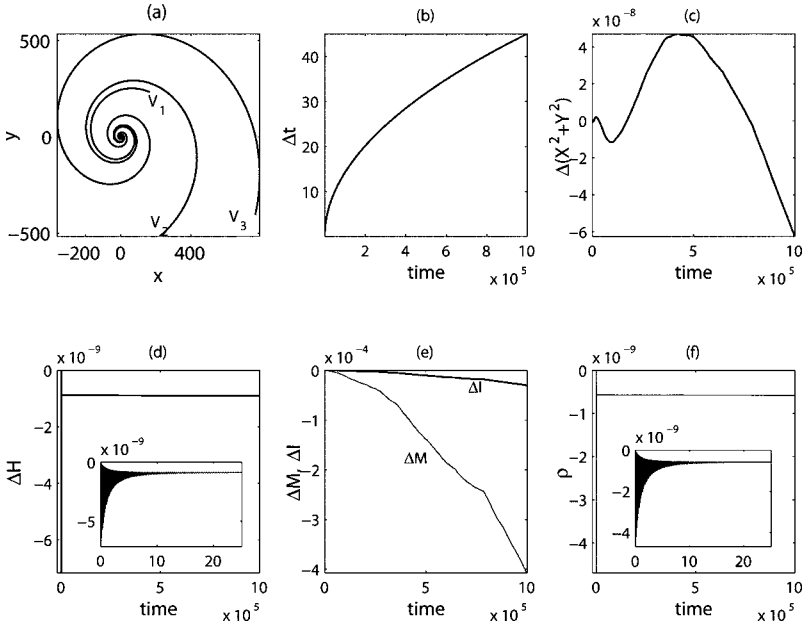

FIG. 8. (a) Orbits for the self-similar expansion of three point vortex in a time interval $[0,10^6]$ computed using the ZQ4A method. (b)–(f) Evolution of the stepsize of real time and the errors in the invariants (X^2+Y^2), H, I, M, and the ratio l_{12}/l_{13}.

$$\kappa_1\kappa_2 + \kappa_2\kappa_3 + \kappa_3\kappa_1 < 0, \quad \kappa_1 + \kappa_3 = 0, \tag{68}$$

(a hyperbolic especial case in the classification by Tvantzis-Ting [25]). The trajectory of this system for the initial value

$$\boldsymbol{q}_0 = (-0.4444,\ 0.5556,\ 0.4617,\ 0,\ 0,\ 0.7348), \tag{69}$$

is contained in a bounded region. The pair of vortices (V_2, V_3) move in a quasiperiodic way approaching and moving away from the vortex V_1 [see Fig. 9(a)]. The energy error for the numerical solution given by ZQ4A in the interval $t \in [0,10^3]$ shows an oscillating behavior [Fig. 9(c)]. The evolution of the error in the other first integrals is shown in Fig. 9(d).

As for the efficiency of the ZQ4A method applied to the considered model, Fig. 7(c) shows the maximum energy error as a function of time for the solution obtained with ZQ4

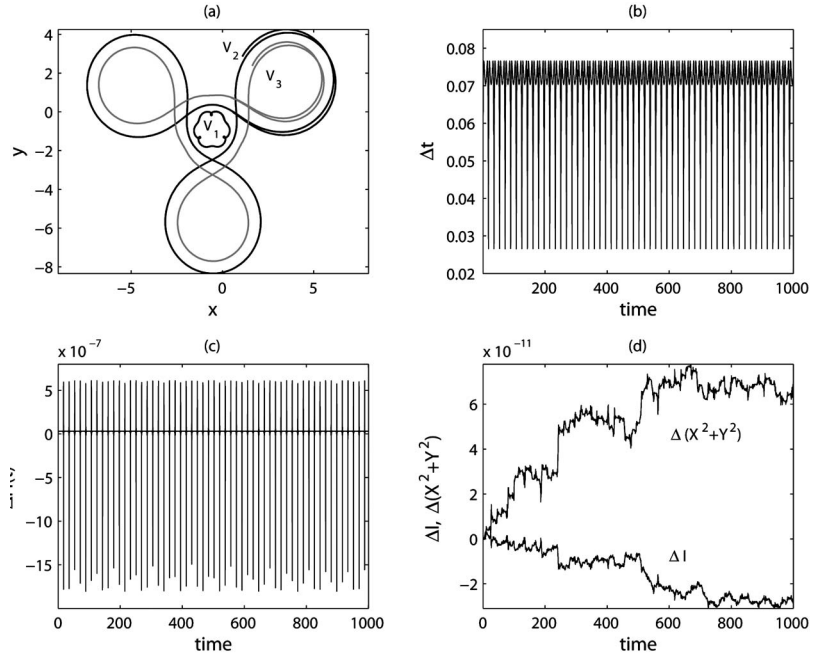

FIG. 9. (a) Orbits of three vortices moving in a bounded region in the time interval $[0,10^3]$ computed using the adaptive integrator ZQ4A (only the segment corresponding to the interval $[0,10^3/15]$) has been plotted. (b) Stepsize of real time as a function of time. (c) Energy error. (e) Errors ΔI and $\Delta(X^2+Y^2)$.

and ZQ4A using the scaling functions $g(\boldsymbol{q})=d(V_1,C)^{3/2}$ and $g(\boldsymbol{q})=\|(\dot{q}_1,\dot{q}_4)\|$. Again the scaling function based on the distance of a vortex to the center of vorticity gives the best results.

VI. CONCLUDING REMARKS

From the explicit symplectic Zhan-Qin scheme for the N-vortex problem, one may construct an adapted explicit method which preserves the reversion symmetry of the dynamical system under a reflection with respect to the Ox axis. In the special problem of the exchange scattering of vortices, to describe the expected symmetry of the orbit it is useful to consider an involution σ composed of a reflection and an exchange of the labels of two vortices. This adaptive method is not σ-reversible. However, a method with this property may be obtained using the Scovel projection and the method so obtained for the three-vortex problem has a good behavior of the energy error for each splitting of the Hamiltonian. The efficiency of the adaptive method ZQ4A is greater than that of the fixed stepsize method ZQ4 for the various models discussed in this paper and depends on the scaling function used in the implementation of the method.

ACKNOWLEDGMENTS

This work was partially supported by JCyL Project No. VA065A05.

APPENDIX A: SOLUTION OF THE TWO-VORTEX PROBLEM

The solution of the differential system $\dot{\boldsymbol{q}}=\mathbb{B}\,\mathrm{grad}\,H_a$, may be expressed through a matrix:

$$\varphi_t^{[a]}=\mathbf{1}+A_{[a]}, \tag{A1}$$

where $\mathbf{1}$ represents the unit $(2N\times 2N)$ matrix and H_a is the Hamiltonian corresponding to a pair of vortices with strengths κ_i and κ_j. In this case $A_{[a]}$ is a matrix whose nonvanishing components are shown in the following array:

$$\begin{array}{c} \\ i \\ j \\ i+N \\ j+N \end{array}\begin{array}{c} \begin{array}{cccccccc} \quad i & & j & & i+N & & j+N & \end{array} \\ \begin{pmatrix} \cdots & a_1 & \cdots & a_2 & \cdots & -b_1 & \cdots & b_1 & \cdots \\ \cdots & a_3 & \cdots & a_4 & \cdots & b_2 & \cdots & -b_2 & \cdots \\ \cdots & b_1 & \cdots & -b_1 & \cdots & a_1 & \cdots & a_2 & \cdots \\ \cdots & -b_2 & \cdots & b_2 & \cdots & a_3 & \cdots & a_4 & \cdots \end{pmatrix} \end{array}, \tag{A2}$$

where a_k and b_k are time functions defined as follows:

$$a_1 := k_{ij}+k_{ji}c_{ij}-1, \quad a_2 := k_{ji}(1-c_{ij}),$$

$$a_3 := k_{ij}(1-c_{ij}), \quad a_4 := k_{ji}+k_{ij}c_{ij}-1, \tag{A3}$$

$$b_1 := k_{ji}s_{ij}, \quad b_2 := k_{ij}s_{ij}, \tag{A4}$$

if $\kappa_a+\kappa_b\neq 0$, and

$$a_1 := 0, \quad a_2 := 0, \quad b_1 := K_j t,$$

$$a_3 := 0, \quad a_4 := 0, \quad b_2 := K_i t, \tag{A5}$$

if $\kappa_a+\kappa_b=0$. In (A3) and (A5) the following notation has been employed:

$$K_i := \frac{\kappa_i}{2\pi r_{ij}^2}, \quad K_{ij}=K_i+K_j, \tag{A6}$$

$$s_{ij}(t) := \sin(K_{ij}t), \quad c_{ij}(t) := \cos(K_{ij}t), \tag{A7}$$

$$k_{ij} := \frac{\kappa_i}{\kappa_i+\kappa_j}, \quad k_{ji} := \frac{\kappa_j}{\kappa_i+\kappa_j}. \tag{A8}$$

APPENDIX B: ENERGY ERROR AND SPLITTING METHODS

In the backward error analysis for symplectic methods $q_{n+1}=\Psi_h(q_n)$ with fixed stepsize, associated to Hamiltonian equations $\dot{q}=\{q,H\}$, the following result is proved (cf. [5]): there exists a Hamiltonian function $\tilde{H}$ such that the mapping

$$\Psi_h=\exp(hD_{\tilde{H}}), \tag{B1}$$

where $D_{\tilde{H}}$ is a differential operator defined in terms of the Poisson bracket associated with (5) as follows:

$$D_{\tilde{H}}F := \{F,G\}, \tag{B2}$$

may be considered as the flow map of the equation $\dot{q} = \{q,\tilde{H}\}$ with time h. Furthermore, if the mapping Ψ_h is a method of order n then

$$H = \tilde{H} + O(h^n). \tag{B3}$$

In particular, for a decomposition $H=H_i+H_j+H_k$ and the second order method (15), this method may be interpreted as the exact flow corresponding to a Hamiltonian system whose Hamiltonian function is given by

$$\tilde{H}^{[i,j,k]} = H + \tfrac{1}{12}h^2\tilde{H}_{[2]}^{[i,j,k]} + O(h^4). \tag{B4}$$

For small values of h the leading term in the error $H-\tilde{H}^{[ijk]}$ is $\frac{1}{12}h^2\tilde{H}_{[2]}^{[i,j,k]}$. Then, for each of the possible splittings the behavior of the energy error may be studied through this leading term. Applying the Baker-Campbell-Hausdorff formula one obtains for $\tilde{H}_{[2]}^{[i,j,k]}$ the expression (see [5])

$$\tilde{H}_{[2]}^{[i,j,k]} = \left\{H_i + \frac{1}{2}H_j, \{H_i,H_j\}\right\} + \left\{H_i + H_j + \frac{1}{2}H_k, \{H_i+H_j,H_k\}\right\}. \tag{B5}$$

This approach has been used by Fassò, [31], in the study of the rigid body using splitting methods.

Using an algebraic processor such as Maple, one may compute, for each splitting of H and for every point $\boldsymbol{q}=(q_1,q_2,q_3,q_4,q_5,q_6)$ in the trajectory of the exchange-scattering model, the values of H-$\tilde{H}^{[i,j,k]}$ for the points q and $\sigma(q)=(q_2,q_1,q_3,-q_5,-q_4,-q_6)$, symmetrics with respect to the axis Ox. The following identities hold

$$\tilde{H}_{[2]}^{[a,i,j]}(\sigma(q)) = \tilde{H}_{[2]}^{[a,j,i]}(q),$$

$$\tilde{H}_{[2]}^{[i,a,j]}(\sigma(q)) = \tilde{H}_{[2]}^{[j,a,i]}(q),$$

$$\tilde{H}_{[2]}^{[i,j,a]}(\sigma(q)) = \tilde{H}_{[2]}^{[j,i,a]}(q), \tag{B6}$$

[where (i,j) is an arbitrary permutation of (b,c)], which in the second order of approximation gives account of the properties of mirror symmetry of the solutions corresponding to the indicated pairs of splittings. Also, the identity

$$\tilde{H}_{[2]}^{[i,j,a]}(\sigma(q)) = \tilde{H}_{[2]}^{[i,j,a]}(q), \tag{B7}$$

is satisfied, so the energy error functions for the splitting $[b,c,a]$ and $[c,b,a]$ are equal. The generalization of this argument to adaptive methods and higher order approximation may be developed following the general results which appear, e.g., in [5] Chap. IX.

[1] H. Aref and N. Pomphrey, Phys. Lett. **78**, 297 (1980).
[2] H. Aref and N. Pomphrey, Proc. R. Soc. London, Ser. A **380**, 359 (1982).
[3] L. Kuznetsov and G. M. Zaslavsky, Phys. Rev. E **61**, 3777 (2000).
[4] J. M. Sanz-Serna and M. P. Calvo, *Numerical Hamiltonian Problems* (Chapman and Hall, New York, 1995).
[5] E. Hairer, C. Lubich, and G. Wanner, *Geometric Numerical Integration: Structure Preserving Algorithms for Ordinary Differential Equations* (Springer-Verlag, Berlin, 2002).
[6] B. Leimkuhler and S. Reich, *Simulating Hamiltonian Dynamics* (Cambridge University Press, Cambridge, 2004).
[7] D. I. Pullin and P. G. Saffman, Proc. R. Soc. London, Ser. A **432**, 481 (1991).
[8] S. Boatto and R. T. Pierrehumbert, J. Fluid Mech. **394**, 137 (1999).
[9] C. W. Rowley and J. E. Marsden, Proc. CDC **40**, 1521 (2002).
[10] P. K. Newton and B. Khushalani, J. Turbul. **3**, 1 (2002).
[11] D. Stoffer, Computing **55**, 1 (1995).
[12] M. P. Calvo, M. A. López-Marcos, and J. M. Sanz-Serna, Appl. Numer. Math. **28**, 1 (1998).
[13] W. Huang and B. Leimkuhler, SIAM J. Sci. Comput. (USA) **18**, 239 (1997).
[14] T. Holder, B. Leimkuhler, and S. Reich, Appl. Numer. Math. **39**, 379 (2001).
[15] B. Leimkuhler, Philos. Trans. R. Soc. London, Ser. A **357**, 1101 (1999).
[16] M.-Q. Zhang and M.-Z Qin, Comput. Math. Appl. **26**, 51 (1993).
[17] J. Moser, *Stable and Random Motions in Dynamical Systems* (Princeton University Press, Princeton, 1973).
[18] H. Aref, Phys. Fluids **22**, 393 (1979).
[19] P. K. Newton, *The N-Vortex Problem. Analytical Techniques* (Springer-Verlag, New York, 2001).
[20] P. Hut, J. Makino, and S. Mcmillan, Astrophys. J. Lett. **443**, L93 (1995).
[21] P. G. Saffman, *Vortex Dynamics* (Cambridge University Press, Cambridge, 1992).
[22] G. K. Batchelor, *An Introduction to Fluid Dynamics* (Cambridge University Press, Cambridge, 2000).
[23] H. Yoshida, Phys. Lett. A **150**, 262 (1990).
[24] T. Kuhlbrodt and P. Névir, Meteorol. Atmos. Phys. **73**, 127 (2000).
[25] J. Tavantzis and L. Ting, Phys. Fluids **31**, 1392 (1988).
[26] J. S. W. Lamb and J. A. G. Roberts, Physica D **112**, 1 (1998).
[27] J. L. Synge, Can. J. Math. **1**, 257 (1949).
[28] R. I. Mclachlan and M. Perlmuter, J. Phys. A **37**, L593 (2004).
[29] R. I. McLachlan, G. R. W. Quispel, and G. S. Turner, SIAM (Soc. Ind. Appl. Math.) J. Numer. Anal. **35**, 586 (1998).
[30] R. I. McLachlan and G. R. W. Quispel, Acta Numerica **11**, 341 (2002).
[31] F. Fassò, J. Comput. Phys. **189**, 527 (2003).
[32] A. Kværnø and B. Leimkuhler, SIAM J. Sci. Comput. (USA) **22**, 1016 (2001).